Desalination and Water Treatment
www.deswater.com

doi: 10.5004/dwt.2017.0308

62 (2017) 387–402
February

Synthesis, characterization and adsorption significance of novel composite (chitosan beads loaded nickel-oxide nanoparticles)

Nirav P. Raval[a], Prapti U. Shah[a], Divya G. Ladha[b], Mayur K. Vekariya[b], Poonam M. Wadhwani[b], Nisha K. Shah[b,*]

[a]*Department of Environmental Science, School of Sciences, Gujarat University, Ahmedabad, Gujarat - 380 009, Tel. +91 9904721558; email: nirav.raval90@gmail.com (N.P. Raval), Tel. +91 9558825191; email: prapti.shah1126@gmail.com (P.U. Shah)*
[b]*Department of Chemistry, School of Sciences, Gujarat University, Ahmedabad, Gujarat - 380 009, Tel. +91 9712952953; email: divya.ladha@gmail.com (D.G. Ladha), Tel. +91 9173759551; email: mmv121288@gmail.com (M.K. Vekariya), Tel. +91 8460519967; email: divya.ladha@gmail.com (P.M. Wadhwani), Tel. +91 9825312095; email: nish_chem2004@yahoo.com (N.K. Shah)*

Received 19 March 2016; Accepted 4 July 2016

ABSTRACT

The aim of this work was to first synthesize biocompatible nanocomposite (chitosan beads loaded nickel-oxide nanoparticles) (CTS/NiO NPs) and then study its potential application towards adsorption of anionic azo dye, Congo red (CR), from wastewater. The newly synthesized and characterized NiO nanoparticles were immobilized onto chitosan beads to prepare CTS/NiO NPs, which was characterized by using Scanning Electron Microscopy (SEM), Energy Dispersive X-ray Spectroscopy (EDX) and Fourier Transform Infrared (FT-IR) analysis. The effects of different system variables such as initial dye concentration, contact time, reaction pH, adsorbent dosage and temperature were investigated and based on the results optimal experimental conditions were ascertained. The results revealed that the amount of CR adsorbed on the adsorbent increases with increasing initial dye concentration and by decreasing pH. The Langmuir isotherm was the best-fit adsorption isotherm model for the experimental data obtained from the non-linear chi-square statistic test. Kinetic studies showed that the adsorption of CR followed pseudo-second order kinetics. Thermodynamic studies revealed that the adsorption process was spontaneous and endothermic in nature.

Keywords: Chitosan beads; Nickel oxide; Nanoparticles; Composite; Congo Red

1. Introduction

The term environment has been derived from a French word "Environia" means to surround. According to P. Gisbert "Environment is anything immediately surrounding an object and exerting a direct influence on it [1]." Environmental pollution refers to the introduction of pollutants into the environment that causes adverse change into the nature. Environmental pollution has become a key focus of concern for both developing and developed nations worldwide because both are affected by and suffer from it. Among major three kinds of environmental pollutions i.e., water, air and soil, pollution of water resources is a matter of great concern. A pollutant can be defined as an unwanted substance introduced into the environment that has undesired effects, or adversely affects the usefulness of natural resources. The pollutant materials are generally classified as organic and inorganic substances. The synthetic dyes and heavy metals ions are major pollutant constituents released into the environment every day.

Synthetic dyes are one of the most common constituents of effluents discharged by various industries i.e., textiles, leather, paper, printing, food, cosmetics, paint, pigments, petroleum, solvent, rubber, plastic, pesticide, wood

* Corresponding author.

preserving chemicals and pharmaceutical industries [2,3]. Even very low concentration of dyes can color large water bodies which obstruct light penetration, hinder photosynthetic activity, inhibit the growth of biota and also have a propensity to chelate metal ions which result in micro toxicity to fish and other organisms [4]. Approximately half of all dyes are azo dyes, making them the largest group of synthetic colorants used in textile industries [5]. Congo Red (CR) [1-naphthalene sulfonic acid, 3, 3′- (4, 4′-biphenylenebis (azo)) bis (4-amino-) disodium salt] is the most commonly used benzidine based azo dye. It has a complex chemical structure and high solubility in aqueous solution. It is metabolized to benzidine, a known human carcinogen and exposure to this dye can cause allergic responses [6]. Although CR, a human carcinogen, has been banned in many countries due to health hazards, but it is still widely consumed in several countries [7] and looking upon its harmful effects it has been selected as a model anionic azo dye in this study.

The treatment techniques applied to a broad range of water and wastewater contaminated with dyes include chemical coagulation/flocculation, ozonation, oxidation, photo-degradation, reverse osmosis, electrodialysis, ultrafiltration, ion-exchange, and chemical precipitation [8]. The application of conventional physico-chemical methods has been restricted due to consumption of high energy and extravagant chemicals. In addition these methods generate large amount of toxic sludge, which also create disposal problem. The biological wastewater treatment techniques are also not effective in the treatment of dye containing effluent because of the low biodegradability of dyes [9]. Amongst all these techniques adsorption has become one of the most economical, effective and widely used treatment techniques for the removal of dyes from aqueous solution.

A number of non-conventional, low-cost adsorbents have been used for the adsorption of CR from aqueous solutions such as cattail root [10]; activated carbon prepared from Myrtus communis and Pomegranate [11]; hen feather [12]; rubber seeds (Hevea brasiliensis) [13] and tea waste [14]. However, because of the hydrophobic/anionic surfaces, some of these adsorbents do not have good adsorption capacities. To overcome from such problems many researchers have studied various nanocomposite materials such as magnetic alginate/γ-Fe_2O_3/Cds nanocomposite [15]; carboxymethylcellulose/montmorillonite nanocomposite [16]; α-Fe/Fe_3O_4 nanocomposite [17]; cobalt hybrid/graphene nanocomposite [18]; ZnS/CdS nanocomposite [19] to remove congo red from aqueous solution by adsorption technique. However, preparation of such composites requires grafting by various chemicals as well as addition of surfactants which ultimately adversely affects the environment. Thus, it is essential to develop the more effective and cheaper adsorbents with higher adsorption capacities and minimum environmental effects.

Chitosan is a linear polymer of α (1→4)-linked 2-amino-2-deoxy-β-D-glucopyranose and is easily derived by deacetylation of chitin. It is highly basic polysaccharide having non-toxic, biocompatible and biodegradable nature. In addition, chitosan is an environmentally amiable compound. To keep in mind these applications of chitosan a number of different chitosan composites such as N,O-carboxymethyl chitosan/montmorillonite nanocomposite [20]; chitosan/montmorillonite nanocomposite [21]; chitosan/organo-montmorillonite nanocomposite [22]; hydroxyapatite/chitosan composite [23] were prepared and used to remove CR. Nickel oxide (NiO) is an important transition metal oxide which can be employed in various fields due to its chemical and thermal stability and environmental benignity [24,25].

To the best of our knowledge, adsorption of CR dye by Chitosan/NiO nanoparticles (CTS/NiO NPs) has not yet been reported. Therefore, the aim of the present study was to synthesize nanocomposite with a simple method and characterize by TEM, SEM, EDX and FT-IR, and then the application of the nanocomposite for the removal of CR from aqueous solutions was investigated by the influence of different adsorption parameters, such as solution pH, initial dye concentration, contact time between adsorbate and adsorbent, adsorbent dosage and temperature. In addition, the equilibrium isotherms, adsorption kinetics and thermodynamics studies were also carried out.

2. Experimental

2.1. Materials and methods

The dye, Congo Red (C.I.: 22120, MW: 696.68, Molecular formula: $C_{32}H_{22}N_6Na_2O_6S_2$, λ_{max}: 497 nm), Chitosan powder and other reagents used in this work were purchased from ACS Chemicals Pvt. Ltd. and used as such without further purification. All reagents used in this study were of analytical reagent grade. Deionized and distilled water was used to prepare all the solutions. Aqueous 1 M NaOH and 1 M HCl solutions were prepared from stock HCl and NaOH. The initial pH was adjusted to the required value using NaOH or HCl solutions prior to addition of the adsorbent.

2.2. Preparation of NiO nano-particles

The synthesis of Nickel oxide nanoparticles (NiO NPs) was described in the previous literature [26,27]. Briefly, the synthesis of NiO NPs was performed in two steps. The first step consisted of the homogeneous precipitation method, in which the precursor of the nano-NiO was synthesized. Where 1 g of nickel nitrate hexahydrate [$Ni(NO_3)_2.6H_2O$] and 4 g of sodium hydrogen carbonate ($NaHCO_3$) were accurately weighed and dissolved in 40 mL of distilled water in a separate container. The solution of $NaHCO_3$ was added drop by drop to the $Ni(NO_3)_2.6H_2O$ solution, which was stirred with a magnetic stirrer at room temperature until a homogeneous solution was obtained. The mixture was then transferred to a round bottom flask, sealed, and the temperature was maintained at 80°C for 1 h in a heating mantle. Then, the solution was filtered and thoroughly washed with distilled water to remove the possibly adsorbed ions and chemicals. In the second step, the collected product was further heated at 500°C for 2 h to obtain the dark colored NiO NPs.

2.3. Synthesis of NiO NPs loaded CTS beads

Chitosan powder was dissolved in 1% (v/v) acetic acid solution to produce a viscous solution with 1% (w/v) chitosan. In this viscous chitosan solution 0.5 g of NiO NPs were added and the solution was stirred for 1 h at 50°C. Afterwards the above solution was cooled down and then

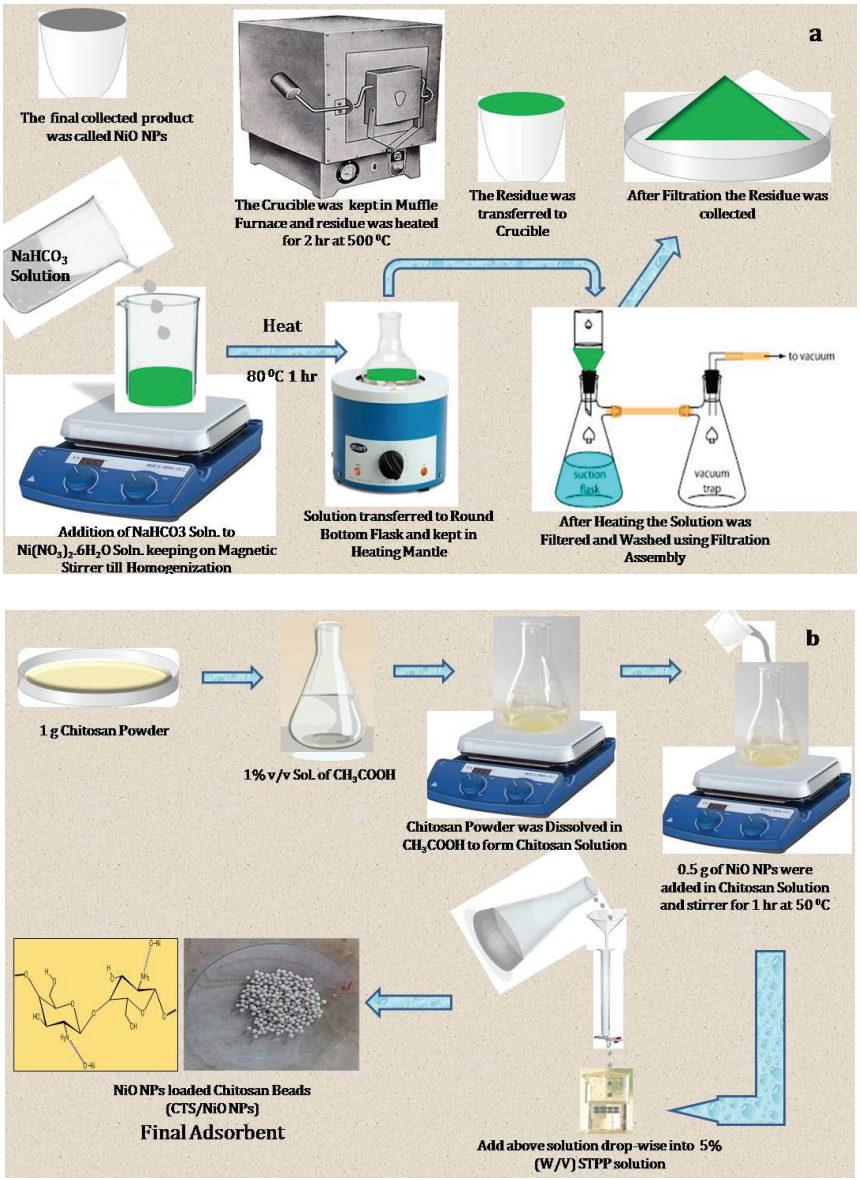

Fig. 1. Synthetic pathways for nickel oxide nanoparticles (a) and chitosan beads loaded nickel oxide nanoparticles (b).

added drop-wise into 100 mL of 5% (w/v) sodium tripolyphosphate (STPP) solution, which neutralized the acetic acid within the chitosan gel and thereby coagulated this gel to spherical uniform beads loaded with NiO NPs. The chitosan beads loaded NiO NPs were filtered rinsed with distilled water and dried under vacuum and can be characterized and used as an adsorbent. Figs. 1(a),(b) presented the synthetic pathways for nickel oxide nanoparticles and chitosan beads loaded nickel oxide nanoparticles, respectively.

2.4. Instrumentation

Transmission electron microscopic (TEM) images of NiO NPs were taken with a Tecnai 20 (Philips, Holland) electron microscope, the sample was dispersed in aqueous ethanol by ultrasonic stirring in order to analyze the structure and morphology of the samples. The surface morphology of NiO NPs and CTS/NiO NPs were studied by using Nova Nano FEG-SEM 450 spectrophotometer at an accelerating voltage of 20 kV attached with an X-ray energy dispersive spectrometer TEAM EDS (EDAX Inc. USA). FT–IR spectra were recorded from 400 to 4,000 cm^{-1} with a Shimadzu-8400S FT-IR spectrophotometer using the KBr pellet technique.

A double beam UV-Visible spectrophotometer (Jasco V–630) was used for determination of CR concentration in the supernatant solutions before and after adsorption. The aqueous pH measurements were carried out using Equip-Tronics pH meter (Digital pH meter Model No.: EQ-615).

2.5. Batch adsorption experiments

A stock solution (1,000 mg/L) of CR dye was prepared by dissolving an appropriate amount of dye in double distilled water, which was further diluted to obtain desired

concentrations. i.e., 25–200 mg/L. Batch adsorption experiments were carried out to investigate the effect of initial dye concentration, contact time, pH, adsorbent dose, and temperature on the adsorption of CR onto CTS/NiO NPs by varying the parameters under study and keeping other parameters constant. In each experiment pre-weighed amount of adsorbent was added to 100 mL of dye solution taken in a 250 mL of conical flask and the pH was adjusted by using 0.1 M NaOH or 0.1 M HCl. The resulting solution was agitated at 120 rpm on a stirrer at constant temperature and centrifuged (Remi Research centrifuge). The dye concentration in supernatant solution were determined at characteristic wavelength (λ_{max} = 497 nm) by double beam UV–visible spectrophotometer.

The removal percentage (R %) of CR was calculated by following expression:

$$R\% = \frac{(C_0 - C_e)}{C_0} \times 100\% \quad (1)$$

The amount of CR adsorbed (mg/g) was calculated based on a following mass balance equation:

$$q_e = \frac{(C_o - C_e)V}{W} \quad (2)$$

where q_e (mg/g) is the equilibrium adsorption capacity per gram dry weight of the adsorbent; C_0(mg/L) is the initial concentration of CR in the solution; C_e(mg/L) is the equilibrium concentration of CR in the solution; V (mL) is the volume of the dye solution; W (mg) is the dry weight of the adsorbent.

2.6. Desorption and regeneration experiments

In order to make the adsorption process economically more feasible, the desorption efficiency and regeneration potential of adsorbent was studied by repeated desorption/adsorption cycles. Desorption studies were carried out by mixing 100 mg of the CTS/NiO NPs beads with 100 mL of the dye solutions (100 mg/L). The mixture was shaken for 3 h at 120 rpm under room temperature (35°C). The composite was collected and washed several times with distilled water to remove unabsorbed CR. Further, dye loaded beads were regenerated in 100 mL of alcohol solution on a rotary shaker at 120 rpm, the concentrations of CR in the elutes were determined to investigate the desorption efficiency, and then it was washed with distilled water until a neutral pH was obtained. The regenerated adsorbent was reused in the next cycle of adsorption experiment.

3. Results and discussion

3.1. Physicochemical characterization

3.1.1. Transmission electron microscope study (TEM)

The size and morphology of NiO nanoparticles has been established by the transmission electron microscopic (TEM) studies. Fig. 2 shows the TEM images of the NiO nanoparticles. The TEM image (Fig. 2(a)) shows the presence of dense agglomerates. The particles have a spherical shape, and their distribution is not uniform. TEM image (Fig. 2(b)) shows the

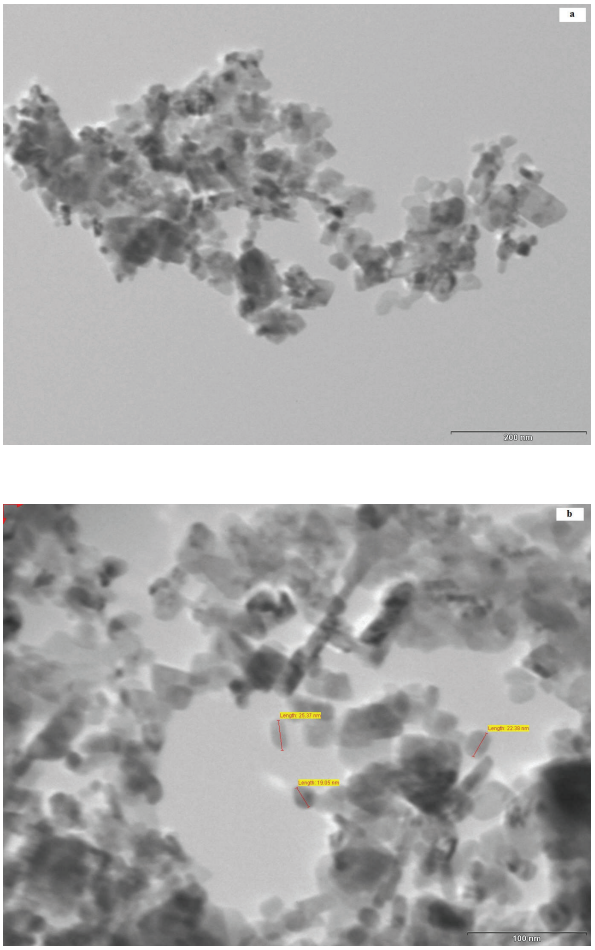

Fig. 2. TEM images of NiO NPs.

NiO nanoparticles have spherical shapes with an average size of 25 nm.

3.1.2. Scanning electron microscope study (SEM)

SEM investigations at different magnifications were carried out to study the morphological features and surface characteristics of (i) NiO NPs and (ii) CTS/NiO NPs before and after CR adsorption, and results are illustrated in Figs. 3(a)–(c).

In Fig. 3(a) the NiO NPs were mostly found as irregular spherical shape. Some particles with agglomerated surfaces were also observed. It has been observed from Fig. 3(b) as well as from the EDX spectra of Fig. 4(b) that the NiO NPs were successfully assimilated with CTS beads. The surface of the CTS/NiO NPs before CR adsorption consists of polymeric network with uneven pores, which becomes even, smooth and non-porous after dye adsorption as examined in Fig. 3(c).

3.1.3. Energy dispersive X-ray microanalysis studies (EDAX)

Figs. 4(a)–(c) shows the Energy Dispersive X-ray (EDX) spectra of NiO NPs, CTS/NiO NPs and dye loaded CTS/NiO NPs, respectively. As illustrated in Fig. 4(b), EDX

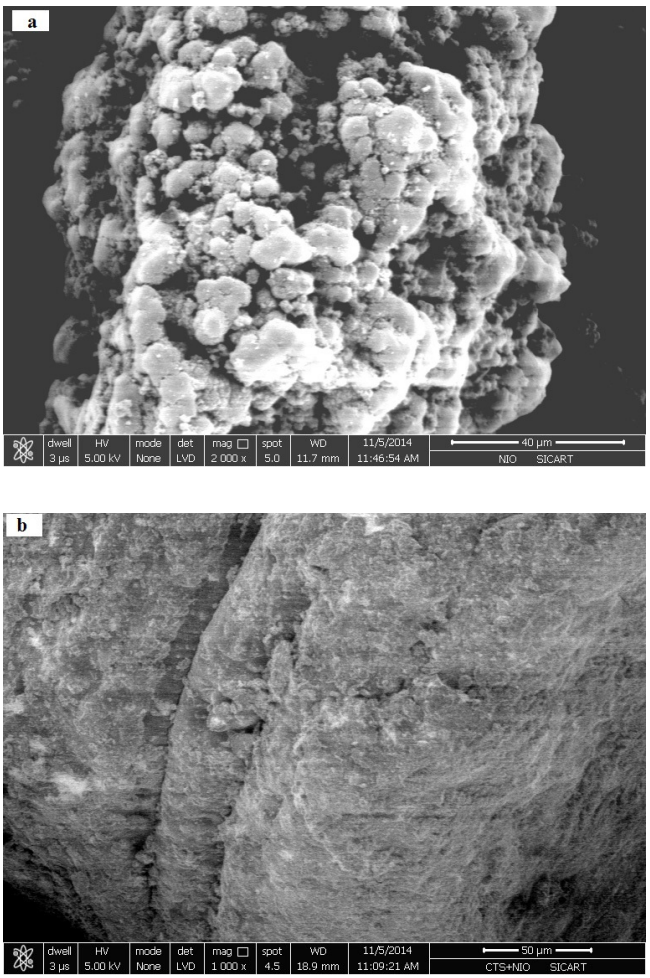

Fig. 3. SEM images of NiO NPs (a); CTS/NiO NPs (b) and CR dye adsorbed CTS/NiO NPs (c).

results showed that the content of nickel on the CTS beads was 25.28 Weight % and 7.88 Atomic %, respectively, which revealed that NiO NPs were successfully incorporated with the CTS beads (Elemental composition (%) shown in the Supplementary Material).

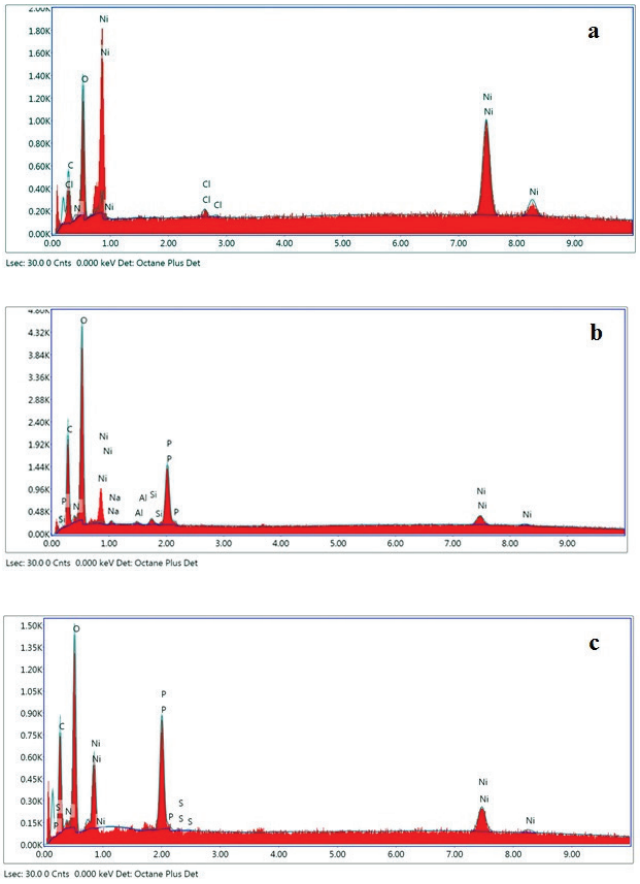

Fig. 4. Energy Dispersive X-ray (EDX) spectra of NiO NPs (a); CTS/NiO NPs (b) CR dye adsorbed CTS/NiO NPs (c).

3.1.4. Fourier transform infrared spectroscopic study (FT-IR)

The surface groups of the adsorbents, which are responsible for the dye adsorption can be examined and identified by using FT-IR data. The presence of characteristic peaks and active sites of the adsorbents were confirmed with the FT-IR spectra. In order to study the formation of Nickel-oxide nanoparticles and CTS/NiO NPs the FT-IR spectra of CTS beads (a), NiO NPs (b) and CTS/NiO NPs (c) were shown in Fig. 5. The characteristic peaks in Fig. 5 confirm the formation of nanoparticles and composite.

As shown in Fig. 5(b) the broad absorption band centered at 3,445.46 cm^{-1} was attributable to the O–H bond stretching vibrations, and the band near 1,635.48 cm^{-1} was assigned to H–O–H bending vibrations. This provided the evidence for the water of hydration in the structure, and it also implied the presence of hydroxyl in the structure. The strong absorption band around 421.33 cm^{-1} was assigned to Ni–O stretching vibration, that shows the formation of nanoparticles as compared to the bulk form of NiO in which the bands generally lies between 390 and 403 cm^{-1} [28].

The wide peak at 3,431.13 cm^{-1}, corresponding to the stretching vibration of hydroxyl, amino and amide groups, moved noticeably to lower wave numbers 3,188.11 cm^{-1} and became broader, which indicated the strong interaction between these groups and NiO NPs. The FT-IR

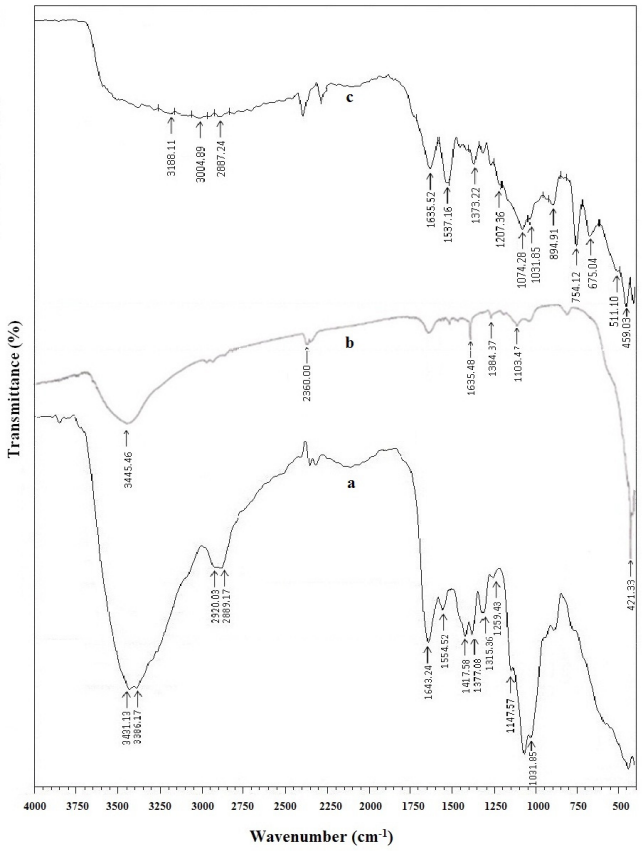

Fig. 5. FT-IR Spectra of CTS Beads (a); NiO NPs (b) and CTS/NiO NPs (c).

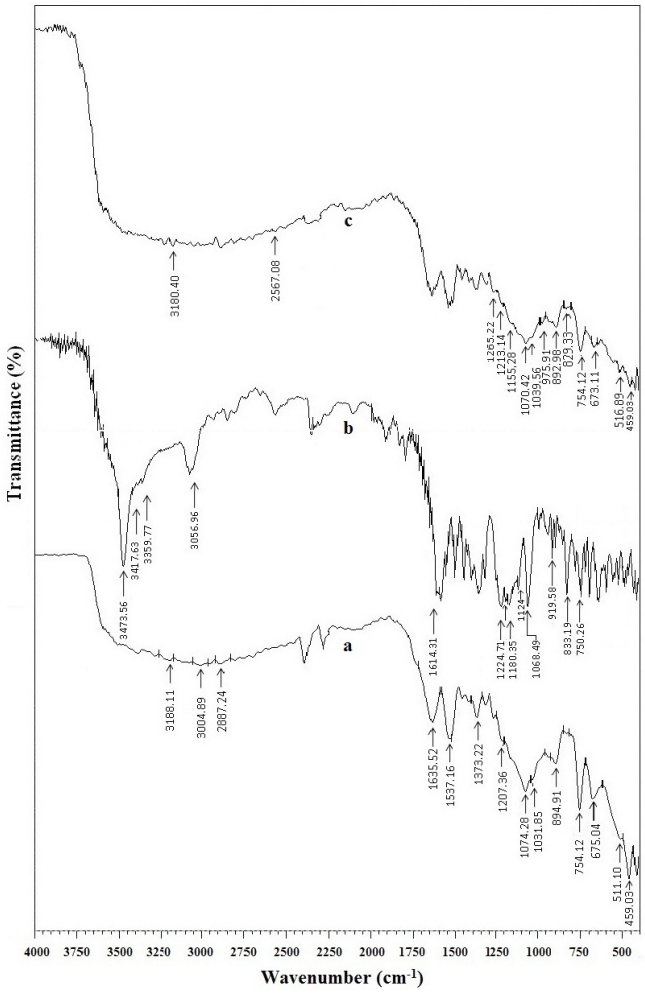

Fig. 6. FT-IR Spectra of CTS/NiO NPs (a); CR dye (b) and CR dye adsorbed CTS/NiO NPs (c).

spectrum of Chitosan itself showed some features of amide groups: amide I and amide II bands at 1,450–1,650 cm^{-1}. The decrease of the band related to primary NH_2 groups at 1,450–1,650 cm^{-1}; 3,300–3,500 cm^{-1}; and 700–800 cm^{-1} is an indicative of NiO NPs immobilization onto the chitosan beads.

FTIR spectra of CTS/NiO NPs (a) and CR dye before (b) and after (c) adsorption are presented in Fig. (6). The major differences are: the absorption band at 3,473.56 cm^{-1} (Fig. 6(b)), corresponding to the stretching vibration of –N–H in the strucure of dye CR, diminishes after adsorption with CTS/NiO NPs (Fig.6(c)).Theband at1,614.31 cm^{-1},assigned to–N=N–stretching (Fig. 6(b)), diminishes after adsorption (Fig. 6(c)). At the same time, the strong bands at 1,224.71, 1,180.35 and 1,068.49 cm^{-1}, attributed to S=O stretching (Fig. 6(b)), also diminish after adsorption (Fig. 6(c)). The results indicated that the NH_2, –N=N– and $–SO_3$ groups of CR were involved in the adsorption process. Furthermore, the bands at 833.19 and 750.26 cm^{-1} assigned to characteristic adsorption of aromatic skeletal groups have also been reduced after adsorption.

3.2. *Effect of pH*

The pH of dye solution significantly affects the complexation of dye molecule with the adsorbent surface. The adsorption of CR was studied in the pH range of 2.0 – 9.0 as shown in Fig. 7. The adsorption capacity of CTS/NiO NPs decreased with increase in solution pH. Tlhe higher adsorption at lower pH was observed mainly because of the electrostatic

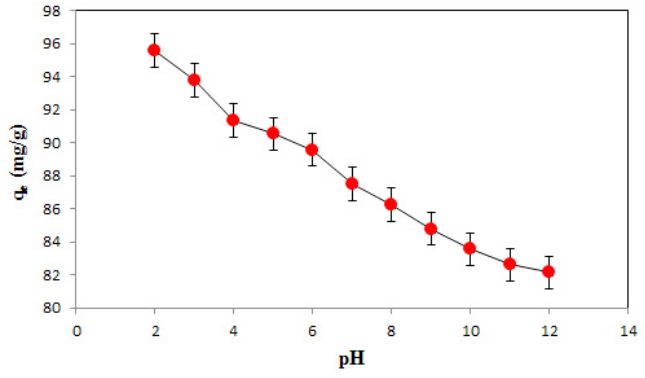

Fig. 7. Effects of pH on the adsorption of CR by CTS/NiO NPs. [C_0 = 100 mg/L; contact time = 60 min; dosage of adsorbent = 100 mg/100 mL; temperature = 308 K; agitation speed = 120 rpm].

interaction between the protonated groups of the adsorbent and the negatively charged SO_3^- groups of the adsorbate. In addition the H-bonding between the oxygen and nitrogen containing functional groups of CR and adsorbent as well as the hydrophobic-hydrophobic interaction between hydrophobic

parts of adsorbate and adsorbent play significant role in the adsorption process. As the pH of the dye solution increases the excessive hydroxyl ions (OH^-) may compete with the dye anions for positively charged sites on the adsorbent and hence a slow reduction in dye uptake was observed. At higher pH adsorption was mainly because of the chemical interaction between adsorbate and adsorbent. Since, CR dye is slightly soluble in water with a pH value of 2.0 as well as its exposure to acid causes color change from red to blue, due to $\pi - \pi^*$ transition of azo group, pH 6.0 was considered as an optimum pH value for adsorption of CR onto CTS/NiO NPs.

3.3. Effect of initial dye concentration and contact time

The adsorption of CR was measured at varying contact times with five different initial dye concentrations. The results obtained at 35°C temperature and 6.0 pH of CR solution are shown in Fig. 8. As shown in figure, with increasing initial dye concentration from 25 to 200 mg/L, the amount of dye adsorption was also increases from 22.51 to 160.36 mg/g. The increase in adsorption capacity at higher initial dye concentration was mainly because of the high driving force for mass transfer at enhanced dye concentration as well as the resistance to the uptake of CR from the solution decreased with increase in CR concentration.

Fig. 8 also indicates that the adsorption of CR is fast at the initial stage of contact with the adsorbent, and then, it becomes slower near the equilibrium. During the initial contact time a large number of vacant surface sites are available for adsorption, and after a lapse of time, aggregation of dye molecules makes it difficult to diffuse deeper into the adsorbent structure at highest energy sites. Based on the results, 60 min contact time was fixed as equilibrium time throughout the adsorption study.

3.4. Effect of adsorbent dosage

The adsorption of CR dye onto CTS/NiO NPs was studied by varying the amount of adsorbent (10–120 mg/100 mL) while keeping the other parameters like initial adsorbate concentration (100 mg/L), contact time between adsorbate and adsorbent (60 min) and temperature (35°C or 308 K) constant. The increase in adsorbent dosage form 10 to 120 mg/100 mL increased the percent removal of adsorbate from 54.97% to 90.08% (shown in Fig. 9), which was attributed to increased adsorbent surface and availability of more adsorption sites. It can be seen from the Fig. 9 that after 100 mg dosage the percent removal of dye remains constant thus further study was carried out by adding 100 mg adsorbent per 100 mL of adsorbate.

Although, the percentage removal of dye increased with increase of adsorbent dose, the equilibrium adsorption capacity (q_e) for CR decreased with increasing amount of adsorbent as depicted in the inset curve (Inset of Fig. 9). This may be due to the decrease in total adsorption surface area available to dye molecules resulting from overlapping or aggregation of adsorption sites.

3.5. Effect of temperature

The adsorption studies were carried out at 25°C, 35°C and 45°C and the results of these experiments are shown in Fig. 10. It was observed that as the temperature increased

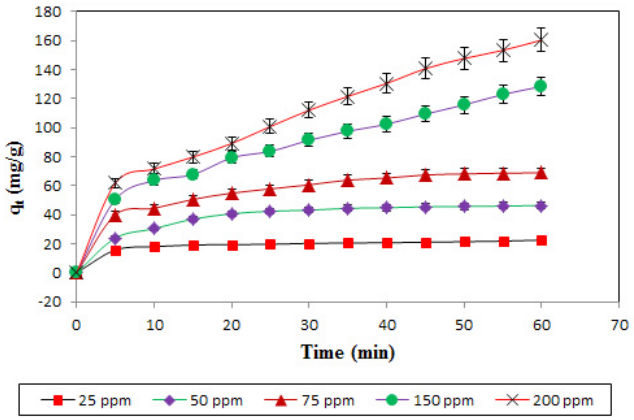

Fig. 8. Effects of initial dye concentrations and contact time on the adsorption of CR by CTS/NiO NPs. [pH = 6.0; dosage of adsorbent = 100 mg/100 mL; temperature = 308 K; agitation speed = 120 rpm].

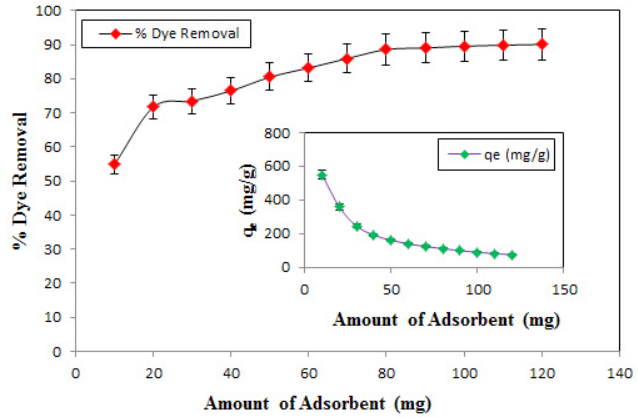

Fig. 9. Effects of amount of adsorbent on the percentage removal of CR by CTS/NiO NPs. [C_0 = 100 mg/L; pH = 6.0; contact time = 60 min; temperature = 308 K; agitation speed = 120 rpm].
Note: Inset of Fig. 9. Effects of amount of adsorbent on the adsorption capacity of CR by CTS/NiO NPs. [C_0 = 100 mg/L; pH = 6.0; contact time = 60 min; temperature = 308 K; agitation speed = 120 rpm].

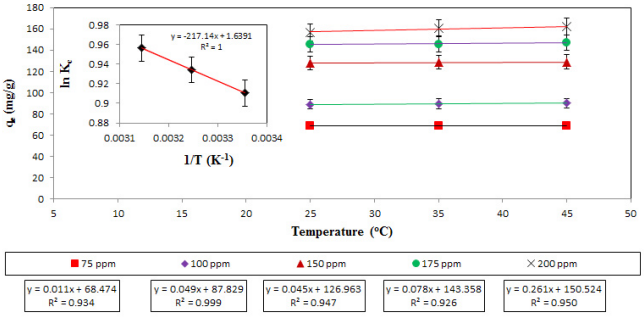

Fig. 10. Effects of temperature for the adsorption of CR onto CTS/NiO NPs. [pH = 6.0; contact time = 60 min; agitation speed = 120 rpm].
Note: Inset of Fig. 10. Van't Hoff plot of *ln* Kc vs. 1/T for the adsorption of CR onto CTS/NiO NPs. [C_0 = 100 mg/L; pH = 6.0; contact time = 60 min; agitation speed = 120 rpm].

the adsorption capacity also increased, which indicated that the process was endothermic in nature. The enhancement in adsorption with temperature may be due to the increase in the mobility of the dye molecule with increase in their kinetic energy and the enhanced rate of intraparticle diffusion of adsorbate with the rise in temperature.

3.6. Equilibrium adsorption isotherms

Adsorption isotherms describe how the adsorbate interacts with adsorbent and provide comprehensive understanding about the nature of the interaction. Isotherms help to provide information about the optimum use of adsorbents. So, in order to optimize the design of an adsorption system to remove dye from solutions, it is essential to establish the most appropriate correlation for the equilibrium curve [29]. The most widely used isotherm models for solid-liquid adsorption are the Langmuir and Freundlich. The equilibrium data were analyzed using these two isotherm models.

The Langmuir model assumes that the each adsorbate molecule is located at specific homogenous sites within the adsorbent. Thus, it predicts the formation of a monolayer of the adsorbate on the homogenous adsorbent surface and does not consider surface heterogeneity of the adsorbent. The linear form of the Langmuir adsorption isotherm [30] is represented as:

$$\frac{C_e}{q_e} = \frac{1}{K_L} + \frac{a_L}{K_L} \cdot C_e \tag{3}$$

where C_e(mg/L) is the equilibrium concentration of the CR in the solution. q_e(mg/g) is the equilibrium adsorption capacity per gram dry weight of the adsorbent corresponding to complete coverage of the adsorptive sites. a_L (L/mg) and K_L (L/g) are the Langmuir isotherm constants. The values of a_L and K_L were calculated from the slope and intercept of the plot of $\frac{c_e}{q_e} vs \cdot c_e$. The parameters of the Langmuir equation were calculated and given in Table 1.

The maximum adsorption capacities of CR by CTS/NiO NPs at 25°C, 35°C and 45°C were 227.3, 232.6 and 238.1 mg/g, respectively, indicating that increasing temperature induced a higher maximum adsorption capacity.

The maximum monolayer concentration of CR on different adsorbents reported elsewhere were also compared with the present study and shown in Table 2.

The essential characteristic feature of Langmuir isotherm can be expressed in terms of "R_L", a dimensionless constant referred to as "separation factor" or "equilibrium parameter". The value of R_L is calculated using the following equation:

$$R_L = \frac{1}{(1 + a_L \cdot C_0)} \tag{4}$$

The R_L value indicates whether the adsorption is unfavorable ($R_L > 1$), linear ($R_L = 1$), favorable ($0 < R_L < 1$) or irreversible ($R_L = 0$) [31]. The values of R_L in this study are listed in Table 1 and all are between 0 and 1, revealing that CTS/NiO NPs is a favorable adsorbent for CR removal, especially at lower CR concentrations.

Freundlich adsorption isotherm [32] defines the adsorption onto the adsorbent with heterogeneous surface. The linear form of Freundlich isotherm model is as follows:

$$\log q_e = \log K_F + \frac{1}{n} \log C_e \tag{5}$$

where K_F ($mg^{1-1/n}$ $L^{1/n}$/g) is the Freundlich adsorption isotherm constant, relating to the extent of adsorption. n (g/L) is the Freundlich exponent. A value for $1/n$ below 1 indicates a normal Langmuir isotherm while $1/n$ above 1 is indicative of cooperative adsorption.

The values of K_F and $1/n$ are calculated from the slope and intercept of the plot of log $q_e$vs. log C_e and were listed in Table 1. Both the plots of Langmuir (a) and Freundlich (b) isotherms have been presented in Fig. 11.

3.7. Error analysis

In the single component isotherm studies, the optimization procedure requires an error function to be defined in order to be able to evaluate the best fit of the isotherm equation to the experimental equilibrium data. In this study, linear coefficient of determination (R^2) and a non-linear Chi-square test (χ^2) were performed for both the isotherms.

The Chi-square test statistics is basically the sum of the squares of the differences between the experimental data and the data obtained by calculating from models, with each squared difference divided by the corresponding data obtained by calculating from models. The mathematical equation can be represented as:

Table 1
Constants for equilibrium isotherm models with error analysis values for CTS/NiO NPs

Experimental conditions	Adsorption isotherm parameters								
	Langmuir					Freundlich			
	q_m (mg/g)	K_L (L/g)	R_L	R^2	χ^2	K_F ($mg^{1-n}.L^n$/g)	$1/n$	R^2	χ^2
T = 298 K	227.3	12.79	0.082 – 0.416	0.969	3.162	16.48	0.652	0.931	16.28
T = 308 K	232.6	13.35	0.080 – 0.411	0.961	3.803	17.46	0.644	0.928	13.31
T = 318 K	238.1	13.81	0.079 – 0.408	0.967	2.943	17.66	0.653	0.936	12.92

Table 2
Comparison of maximum monolayer adsorption capacity of various absorbents for CR removal

Sr. No.	Adsorbents	q_{max} (mg/g)	Kinetic study	Isotherm study	Thermodynamic study	Contact time	Adsorbent dosage	References
1	Chitosan beads loaded nickel-oxide nanoparticles (CTS/NiO NPs)	238.1	Pseudo 2nd order	Langmuir	Endothermic	60 min	100 mg/100 mL	Present Study
2	Hierarchical NiO architectures	223.8	Pseudo 2nd order	Freundlich	–	120 min	0.02 g/50 mL	[39]
3	Modified xanthan gum/silica hybrid nanocomposite	209.2	Pseudo 2nd order	Langmuir	Endothermic	150 min	50 mg/25 mL	[40]
4	Chitosan beads	166.67	Pseudo 2nd order	Langmuir	–	90 min	0.1 g/100 mL	[41]
5	Carboxymethyl cellulose/montmorillonite nanocomposite	161.1	Pseudo 2nd order	Langmuir	–	360 min	–	[16]
6	Polyethyleneimine-modified wheat straw	118.0	Pseudo 2nd order	Langmuir	Endothermic	–	10.0 g/L	[42]
7	Chitin (CH) Beads	112.36	Pseudo 2nd order	Langmuir	–	90 min	0.1 g/100 mL	[41]
8	γ - Fe_2O_3/C nanocomposite	105.30	–	Langmuir	–	120 min	0.5 g L^{-1}	[43]
9	γ-Al_2O_3/$Ni_{0.5}Zn_{0.5}Fe_2O_4$ microfibers	75.52	Pseudo 2nd order	Temkin	–	180 min	2.5 g L^{-1}	[44]
10	N,O-carboxymethyl chitosan/montmorillonite nanocomposite	74.24	Pseudo 2nd order	Langmuir	Endothermic	480 min	0.05 g/25 mL	[20]
11	Magnetic cellulose/Fe_3O_4/activated carbon composite	66.09	Pseudo 2nd order	Langmuir	Exothermic	600 min	1.0 g L^{-1}	[45]
12	Magnetic composite (chitosan coated magnetic Fe_3O_4 particle)	56.66	Pseudo 2nd order	Langmuir	Endothermic	–	–	[46]
13	Chitosan/montmorillonite nanocomposite	54.52	Pseudo 2nd order	Langmuir	Endothermic	480 min	0.1 g/25 mL	[21]
14	Fe_3O_4/C nanocomposite	48.10	–	Langmuir	–	120 min	0.5 g L^{-1}	[43]
15	Magnetic Fe_3O_4@ graphene composite (FGC)	33.66	Pseudo 2nd order	Langmuir	–	30 min	10 mg/25 mL	[47]
16	Polyaniline-Montmorrillonite Composite	25.1	–	Freundlich	Endothermic	60 min	50 mg/50 mL	[48]

$$\chi^2 = \sum \frac{(q_{e(\exp)} - q_{e(cal)})^2}{q_{e(cal)}} \quad (6)$$

where, $q_{e(\exp)}$ (mg/g) is the experimental data of the equilibrium capacity; $q_{e(cal)}$(mg/g) is the equilibrium capacity obtained by calculating from the model. If data from the model are similar to the experimental data, χ^2 will be a smaller number, and if they differ, χ^2 will be a bigger number. Therefore it is necessary to analyze the data using the non-linear Chi-square test to confirm the best fit isotherm for this adsorption system [33].

The results of the linear coefficient of determination (R^2) and a non-linear Chi-square test (χ^2) for two adsorption isotherms indicated that the Langmuir isotherm model appeared to be the best fitting model for adsorption of CR onto CTS/NiO NPs.

3.8. Adsorption kinetics

Study of sorption kinetics provides valuable insights into the reaction pathways and in turn controls the residence time of adsorbate uptake at the solid-solution interface. In addition kinetics study is helpful for selecting

optimum operating conditions for the full-scale batch process [34]. Therefore, several kinetic models including the pseudo-first-order equation, pseudo-second-order equation and intraparticle diffusion model were applied to the experimental data obtained.

The linear equations for the applied models were:
Pseudo-first-order model:

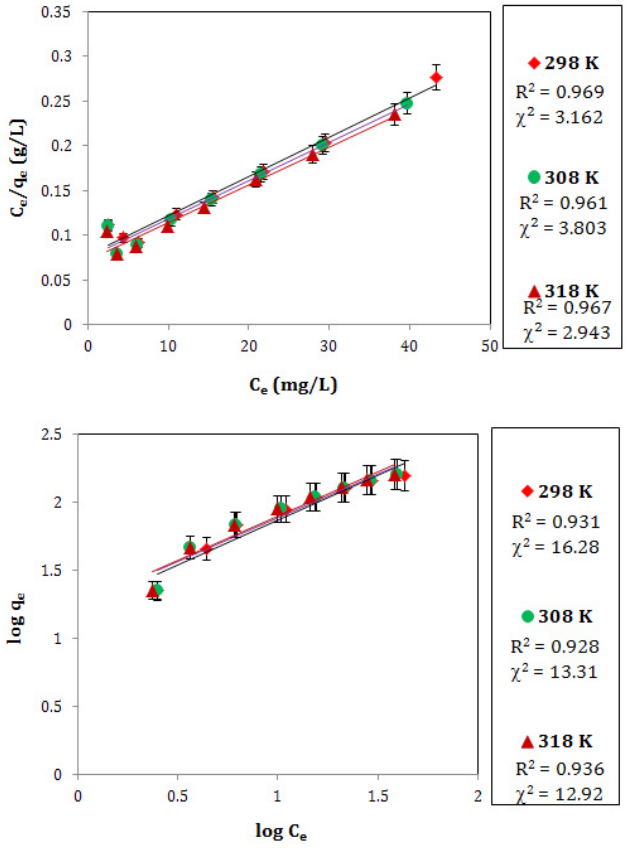

Fig. 11. Langmuir (a) and Freundlich (b) isotherm plots for the adsorption of CR onto CTS/NiO NPs. [pH = 6.0; contact time = 60 min; dosage of adsorbent = 100 mg/100 mL; agitation speed = 120 rpm].

$$\log(q_e - q_t) = \log q_e - \frac{k_1}{2.303}t \quad (7)$$

Pseudo-second-order model:

$$\frac{t}{q_t} = \frac{1}{k_2 q_e^2} + \frac{t}{q_e} \quad (8)$$

Intraparticle-diffusion model:

$$q_t = K_{id}t^{1/2} + I \quad (9)$$

where q_e(mg/g) and q_t (mg/g) are the amounts of dye adsorbed on adsorbent at equilibrium and at time t, respectively, k_1 (1/min) and k_2 (g/mg min) are the rate constants of pseudo-first-order and pseudo-second-order kinetic models. K_{id} is the intraparticle diffusion rate constant (mg/g min$^{1/2}$) and l (mg/g) is the intercept.

The straight-line plots of log (q_e–q_t) vs. t for the pseudo-first-order reaction and the t/q_t vs. t for the pseudo-second-order reaction for the adsorption CR onto CTS/NiO NPs have been investigated toobtain the rate parametersand are given in Table 3. It can be seen that the values of the correlation coefficient for pseudo-second-order rate model were closer to unity as compare to the pseudo-first-order. As shown in Table 3 the values of the rate constant k_2 decreases with increasing initial CR dye concentration because higher dye concentration corresponds to higher surface loading which decreases the diffusion efficiency. The plots of pseudo-first-order and pseudo-second-order were shown in Figs. 12 and 13.

The adsorbate species are most probably transported from the bulk of the solution into the solid phase through intraparticle diffusion/transport process, which is often the rate-limiting step in many adsorption processes. The possibility of intraparticle diffusion was explored by using the intraparticle diffusion model [35], which is commonly expressed by the Eq. (7).

The value of intercept I provides information about the thickness of the boundary layer, the resistance to the external mass transfer increase as the intercept increase. If the intraparticle diffusion is involved in the adsorption process, then a plot of $t^{1/2}$ vs. q_t would result in a linear relationship and

Table 3
Kinetic parameters for the removal of Congo Red by CTS/NiO NPs

Adsorption kinetics rate models	Kinetic parameters (308 K)	Initial concentration of CR dye					
		25 mg/L	50 mg/L	75 mg/L	100 mg/L	150 mg/L	200 mg/L
Pseudo-first-order model	k_1 (1/min)	0.038	0.081	0.090	0.047	0.045	0.049
	$q_{e\,(cal)}$ (mg/g)	7.114	32.73	77.25	90.82	120.98	172.47
	R^2	0.959	0.994	0.918	0.835	0.899	0.923
Pseudo-second-order model	k_2 (g/mg.min)	0.012	0.004	0.002	0.0005	0.0004	0.0002
	$q_{e\,(cal)}$ (mg/g)	23.04	51.02	76.92	108.7	153.8	208.3
	R^2	0.997	0.999	0.997	0.942	0.960	0.945
Intraparticle diffusion model	K_{id} (mg/g.min$^{1/2}$)	1.021	3.748	5.595	9.746	14.001	19.06
	I (mg/g)	14.46	20.43	28.71	11.01	16.37	10.19
	R^2	0.939	0.856	0.973	0.974	0.990	0.984

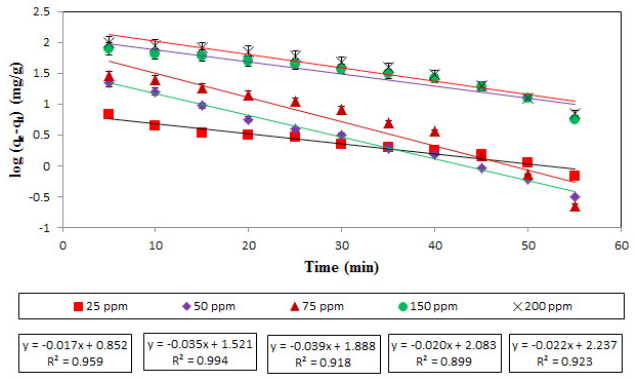

Fig. 12. Pseudo-first-order model for the adsorption of CR onto CTS/NiO NPs. [pH = 6.0; dosage of adsorbent = 100 mg/100 mL; temperature = 308 K; agitation speed = 120 rpm].

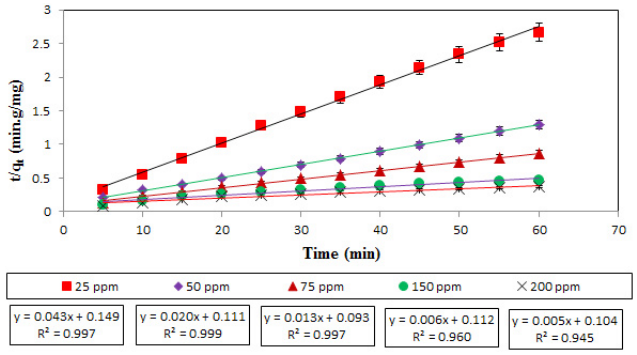

Fig. 13. Pseudo-second-order model for the adsorption of CR onto CTS/NiO NPs. [pH = 6.0; dosage of adsorbent = 100 mg/100 mL; temperature = 308 K; agitation speed = 120 rpm].

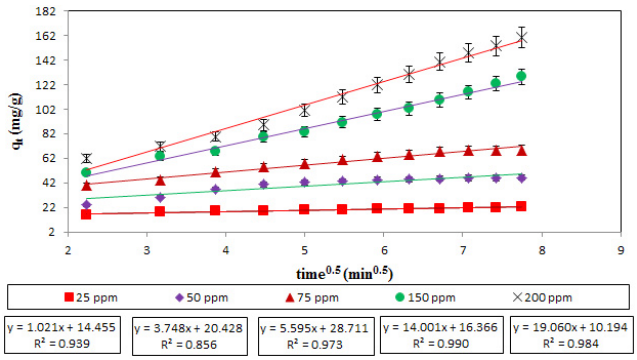

Fig. 14. Intraparticle diffusion model for the adsorption of CR onto CTS/NiO NPs. [pH = 6.0; dosage of adsorbent = 100 mg/100 mL; temperature = 308 K; agitation speed = 120 rpm].

the particle diffusion would be the controlling step if this line passed through the origin. When the plots do not pass through the origin, this is indicative of some degree of boundary layer control and the further show that the intraparticle diffusion is not the only rate-controlling step, but also other processes may control the rate of adsorption, all of which may be operating simultaneously [36]. From Fig. 14 it can be seen that the linear portions of curves do not pass through the origin. This indicates that the intraparticle diffusion is not the sole rate controlling step for the adsorption mechanism of CR onto nanocomposite. The intraparticle diffusion rate constant, K_{id}, were in the range of 1.021 to 19.06 mg/g min$^{1/2}$ and it increase with increase of initial dye concentration. From the above results it may be concluded that surface adsorption and intraparticle diffusion were concurrently operating during the CR and adsorbent interactions [37].

3.9. Thermodynamic study

The thermodynamic parameters such as change in Gibb's free energy (ΔG^o), change in enthalpy (ΔH^o) and change in entropy (ΔS^o) were also studied to understand better the effect of temperature on the adsorption process.

The Gibbs free energy of adsorption $\Delta G°$ is calculated from the following equation:

$$\Delta G° = -RT \ln K_c \tag{10}$$

where K_c is the adsorption equilibrium constant. The value of K_c is calculated from the following equation:

$$K_c = \frac{C_{ae}}{C_e} \tag{11}$$

where C_{ae} is the equilibrium dye concentration on the adsorbent (mg/L) and C_e is the equilibrium dye concentration in solution (mg/L).

Standard enthalpy and Standard entropy of adsorption can be estimated from Van't Hoff equation:

$$\ln K_c = -\frac{\Delta H°}{RT} + \frac{\Delta S°}{R} \tag{12}$$

The value of $\Delta H°$ and $\Delta S°$ were calculated from the slope and intercept of Van't Hoff plot (presented in the inset curve of Fig. 10) of $\ln K_c$ vs. $1/T$ and are shown in Table 4.

The Gibbs free energy demonstrates a spontaneous and favorable adsorption process. The higher negative value reflects a more energetically favorable adsorption. As shown in Table 4, the values of $\Delta H°$ and $\Delta S°$ were positive for adsorption of CR onto CTS/NiO NPs. The important thermodynamic function $\Delta H°$ is very useful whenever there is a differential change occurs in the system. The positive value of $\Delta H°$ indicates that the adsorption process is endothermic in nature and the positive value of $\Delta S°$ showed the increase in degree of freedom or increases the disorder of adsorption process. It also suggests increased randomness during adsorption [38].

3.10. Desorption and regeneration studies

In order to evaluate the possibility of regeneration of composite adsorbent desorption experiments have been performed. The cycles of adsorption/desorption experiments were carried out up to three times. After four cycles, the adsorption capacities of CR dye on adsorbent decreases from 61.59% to 50.32%. This behavior indicates that the adsorbent can be reused successfully three times for the CR adsorption from aqueous solution.

Table 4
The obtained thermodynamic parameters of CR adsorption on CTS/NiO NPs

Sr. No.	Initial CR concentration C_0 (mg/L)	Temperature (*K*)	ΔG° (kJ/mol)	ΔH° (kJ/mol)	ΔS° (kJ/mol/K)	R^2
1	25	298	–5.432	2.784	0.027	0.84
		308	–5.640			
		318	–5.985			
2	50	298	–5.780	8.243	0.047	0.773
		308	–6.500			
		318	–6.716			
3	75	298	–5.933	1.527	0.025	0.944
		308	–6.204			
		318	–6.434			
4	100	298	–5.195	4.158	0.031	1
		308	–5.509			
		318	–5.822			
5	125	298	–4.833	3.264	0.027	0.861
		308	–5.032			
		318	–5.378			
6	150	298	–4.383	1.924	0.021	0.937
		308	–4.567			
		318	–4.807			
7	175	298	–3.949	2.553	0.022	0.914
		308	–4.123			
		318	–4.386			
8	200	298	–3.188	6.390	0.032	0.962
		308	–3.580			
		318	–3.829			

3.11. Mechanism of adsorption

The investigation of adsorption mechanism is an important function to be performed in the dye adsorption study. The possible interactions between adsorbate (congo red dye) and adsorbent (nanocomposite) were hydrogen bonds, electrostatic interaction and availability of larger surface area due to the presence of nanoparticles. Hydroxyl was the major functional groups of nanocomposite which adsorb dye by the formation of hydrogen bond. In addition, presence of carboxyl and amide functional groups adsorbs the dye by electrostatic interaction.

The surfaces of CTS/NiO NPs have the positive charges relevant to metal cations (Ni^{2+}) that can adsorb the anionic CR dye as there are two sulfonate groups in CR molecule. Therefore below the neutral pH, the adsorbent surface is positively charged, and anion adsorption occurs due to electrostatic attractions. Another theory at acidic pH is also existence of hydrogen bonds between adsorbent's hydroxyl groups and sulfonate or amine sites of dye molecule. As the pH of the CR solution increased, an extreme decrease in adsorption took place. Generally at higher pHs, the anion OH^- can compete with anionic sites of CR dye.

4. Conclusions

Novel biocompatible nanocomposite (Chitosan beads loaded nickel oxide nanoparticles) was synthesized, characterized and its adsorption properties were investigated for hazardous anionic azo dye congo red. TEM, SEM, FT-IR and EDX were analyzed, and the results indicate that the nanocomposite has been successfully prepared and further can be used as an adsorbent. Various system variables like pH, adsorbate concentration, contact time, dosage of adsorbents and temperature on adsorption of CR were investigated. The results indicate that the adsorption of CR increases with increasing initial dye concentration, decreasing pH and reaches equilibrium within 60 min of contact time. The adsorption process followed well to the Langmuir adsorption isotherm and the highest adsorption capacity approaches 238.1 mg/g. The thermodynamic parameters calculated from the temperature-dependent isotherms indicate that the adsorption is spontaneous process and endothermic in nature. Further, the pseudo-first-order and second-order kinetic models were used to describe the kinetic data, and the rate constants were evaluated. The experimental data fit well with the second-order kinetic model.

Acknowledgements

The authors gratefully acknowledge the financial assistance provided by the INSPIRE Programme under the Assured Opportunity for Research Careers (AORC) scheme, funded by the Department of Science and Technology (DST)

(Sanction Order No.: DST/INSPIRE Fellowship/2013/66) [IF130088]. The authors also acknowledge SICART (Anand), L. M. College of Pharmacy (Ahmedabad) for providing instrumental facilities and INFLIBNET (Ahmedabad) for e-journals.

Abbreviations

CTS Beads	—	Chitosan Beads
CTS/NiO NPs	—	Chitosan beads loaded nickel oxide nanoparticles
CR	—	Congo red
TEM	—	Transmittance electron microscopy
SEM	—	Scanning electron microscopy
EDX	—	Energy dispersive X-ray spectroscopy
FT–IR	—	Fourier transform Infrared spectroscopy
UV–Vis.	—	Ultraviolet–visible spectrophotometer

Symbols

R %	—	Removal percentage of dye
q_e	—	The equilibrium adsorption capacity of the adsorbent, mg/g
C_0	—	The initial concentration of CR in the solution, mg/L
C_e	—	The equilibrium concentration of CR in the solution, mg/L
V	—	The volume of the solution, mL
W	—	The dry weight of CTS/NiO NPs, mg
t	—	Time (minute)
a_L	—	The Langmuir isotherm constant, L/mg
K_L	—	The Langmuir isotherm constant, L/g.
q_m	—	The monolayer sorption capacity of the nanocomposite, mg/g
R^2	—	The Linear coefficient of determination
R_L	—	Separation factor or Equilibrium parameter (Dimensionless)
K_F	—	The Freundlich adsorption isotherm constant ($mg^{1-1/n}\ L^{1/n}$ / g)
n	—	The Freundlich exponent (g/L)
χ^2	—	A non-linear Chi-square test
$q_{e(exp)}$	—	The experimental data of the equilibrium capacity, mg/g
$q_{e(cal)}$	—	The equilibrium capacity obtained by calculating from the model, mg/g
T	—	Absolute temperature, K
q_t	—	The amounts of dye adsorbed on adsorbent at time t, mg/g
k_1	—	The pseudo-first-order rate constant, (per minute)
k_2	—	The pseudo-second-order rate constant, g/mg.min
K_c	—	The equilibrium constant at temperature T (Dimensionless)
C_{ae}	—	The equilibrium dye concentration on the adsorbent, mg/L
ΔH°	—	Change in Enthalpy, kJ/mol
ΔS°	—	Change in Entropy, J/mol/K
ΔG°	—	Gibbs free energy, kJ/mol
R	—	Universal gas constant, 8.314 J/mol/K

References

[1] G. Pascual, Fundamentals of Sociology, Orient Longman Limited, 1989.
[2] S. Chowdhury, R. Mishra, P. Saha, P. Kushwaha, Adsorption thermodynamics, kinetics and isosteric heat of adsorption of malachite green onto chemically modified rice husk, Desalination, 265 (2011) 159–168.
[3] A. Ergene, K. Ada, S. Tan, H. Katırcıoğlu, Removal of remazol brilliant blue R dye from aqueous solutions by adsorption onto immobilized *Scenedesmus quadricauda*: equilibrium and kinetic modeling studies, Desalination, 249 (2009) 1308–1314.
[4] S. Hajati, M. Ghaedi, F. Karimi, B. Barazesh, R. Sahraei, A. Daneshfar, Competitive adsorption of direct yellow 12 and reactive orange 12 on ZnS:Mn nanoparticles loaded on activated carbon as novel adsorbent, J. Ind. Eng. Chem., 20 (2014) 564–571.
[5] K. Selvam, K. Swaminathan, K.-S. Chae, Decolourization of azo dyes and a dye industry effluent by a white rot fungus Thelephora sp., Bioresour. Technol., 88 (2003) 115–119.
[6] N.P. Raval, P.U. Shah, N.K. Shah, Adsorptive amputation of hazardous azo dye congo red from waste water: a critical review, Environ. Sci. Pollut. Res., 23 (2016) 14810–14853. doi: 10.1007/s11356-016-6970-0
[7] A. Afkhami, R. Moosavi, Adsorptive removal of Congo red, a carcinogenic textile dye, from aqueous solutions by maghemite nanoparticles, J. Hazard. Mater., 174 (2010) 398–403.
[8] G.M. Walker, L. Hansen, J.-A. Hanna, S.J. Allen, Kinetics of a reactive dye adsorption onto dolomitic sorbents, Water Res., 37 (2003) 2081–2089.
[9] S. Chatterjee, D.S. Lee, M.W. Lee, S.H. Woo, Enhanced adsorption of congo red from aqueous solutions by chitosan hydrogel beads impregnated with cetyl trimethyl ammonium bromide, Bioresour. Technol., 100 (2009) 2803–2809.
[10] Z. Hu, H. Chen, F. Ji, S. Yuan, Removal of Congo Red from aqueous solution by cattail root, J. Hazard. Mater., 173 (2010) 292–297.
[11] M. Ghaedi, H. Tavallali, M. Sharifi, S.N. Kokhdan, A. Asghari, Preparation of low cost activated carbon from Myrtus communis and pomegranate and their efficient application for removal of Congo red from aqueous solution, Spectrochim. Acta. A Mol. Biomol. Spectrosc., 86 (2012) 107–114.
[12] A. Mittal, V. Thakur, J. Mittal, H. Vardhan, Process development for the removal of hazardous anionic azo dye Congo red from wastewater by using hen feather as potential adsorbent, Desal. Wat. Treat., 52 (2014) 227–237.
[13] M.A. Zulfikar, H. Setiyanto, Rusnadi, L. Solakhudin, Rubber seeds (*Hevea brasiliensis*): an adsorbent for adsorption of Congo red from aqueous solution, Desal. Wat. Treat., 56 (2014) 2976–2987.
[14] M. Foroughi-Dahr, H. Abolghasemi, M. Esmaili, A. Shojamoradi, H. Fatoorehchi, Adsorption characteristics of congo red from aqueous solution onto tea waste, Chem. Eng. Commun., 202 (2015) 181–193.
[15] R. Jiang, J. Yao, H. Zhu, Y. Fu, Y. Guan, L. Xiao, G. Zeng, Effective decolorization of congo red in aqueous solution by adsorption and photocatalysis using novel magnetic alginate/γ-Fe_2O_3/CdS nanocomposite, Desal. Wat. Treat., 52 (2014) 238–247.
[16] Y.H. Zhao, L. Wang, Adsorption characteristics of congo red from aqueous solution on the carboxymethylcellulose/montmorillonite nanocomposite, Adv. Mater. Res., 450–451 (2012) 769–772.
[17] L. Wang, J. Li, Z. Wang, L. Zhao, Q. Jiang, Low-temperature hydrothermal synthesis of α-Fe/Fe_3O_4 nanocomposite for fast Congo red removal, Dalton Trans., 42 (2013) 2572.
[18] L. Wang, J. Li, C. Mao, L. Zhang, L. Zhao, Q. Jiang, Facile preparation of a cobalt hybrid/graphene nanocomposite by *in situ* chemical reduction: high lithium storage capacity and highly efficient removal of Congo red, Dalton Trans., 42 (2013) 8070.

[19] H.R. Pouretedal, S. Sabzevari, Photodegradation study of congo red, methyl orange, methyl red and methylene blue under simulated solar irradiation catalyzed by ZnS/CdS nanocomposite, Desal. Wat. Treat., 28 (2011) 247–254.
[20] L. Wang, A. Wang, Adsorption behaviors of Congo red on the N,O-carboxymethyl-chitosan/montmorillonite nanocomposite, Chem. Eng. J., 143 (2008) 43–50.
[21] L. Wang, A. Wang, Adsorption characteristics of Congo Red onto the chitosan/montmorillonite nanocomposite, J. Hazard. Mater., 147 (2007) 979–985.
[22] L. Wang, A. Wang, Removal of Congo red from aqueous solution using a chitosan/organo- montmorillonite nanocomposite, J. Chem. Technol. Biotechnol., 82 (2007) 711–720.
[23] H. Hou, R. Zhou, P. Wu, L. Wu, Removal of Congo red dye from aqueous solution with hydroxyapatite/chitosan composite, Chem. Eng. J., 211–212 (2012) 336–342.
[24] A. Wei, B. Liu, H. Zhao, Y. Chen, W. Wang, Y. Ma, H. Yang, S. Liu, Synthesis and formation mechanism of flowerlike architectures assembled from ultrathin NiO nanoflakes and their adsorption to malachite green and acid red in water, Chem. Eng. J., 239 (2014) 141–148.
[25] N.P. Raval, P.U. Shah, N.K. Shah, Adsorptive removal of nickel(II) ions from aqueous environment: a review, J. Environ. Manage., 179 (2016) 1–20. doi: 10.1016/j.jenvman.2016.04.045
[26] P.M. Wadhwani, D.G. Ladha, V.K. Panchal, N.K. Shah, Enhanced corrosion inhibitive effect of p-methoxybenzylidene-4,4′-dimorpholine assembled on nickel oxide nanoparticles for mild steel in acid medium, RSC Adv., 5 (2014) 7098–7111.
[27] P.M. Wadhwani, V.K. Panchal, N.K. Shah, Newly synthesized salicylidene-4,4′-dimorpholine (SDM) assembled on nickel oxide nanoparticles (NiONPs) and its inhibitive effect on mild steel in 2 N hydrochloric acid, Appl. Surf. Sci., 331 (2015) 373–387.
[28] A. Kalam, A.G. Al-Sehemi, A.S. Al-Shihri, G. Du, T. Ahmad, Synthesis and characterization of NiO nanoparticles by thermal decomposition of nickel linoleate and their optical properties, Mater. Charact., 68 (2012) 77–81.
[29] Y.C. Wong, Y.S. Szeto, W.H. Cheung, G. McKay, Adsorption of acid dyes on chitosan—equilibrium isotherm analyses, Process Biochem., 39 (2004) 695–704.
[30] I. Langmuir, The adsorption of gases on plane surfaces of glass, mica and platinum, J. Am. Chem. Soc., 40 (1918) 1361–1403.
[31] C.M. Futalan, C.-C. Kan, M.L. Dalida, K.-J. Hsien, C. Pascua, M.-W. Wan, Comparative and competitive adsorption of copper, lead, and nickel using chitosan immobilized on bentonite, Carbohydr. Polym., 83 (2011) 528–536.
[32] H.M. Freundlich, Over the adsorption in solution, J. Phys. Chem., 57 (1906) 385–470.
[33] P.U. Shah, N.P. Raval, N.K. Shah, Adsorption of copper from an aqueous solution by chemically modified cassava starch, J. Mater. Environ. Sci., 6 (2015) 2573–2582.
[34] N.P. Raval, P.U. Shah, N.K. Shah, Nanoparticles loaded Biopolymer as effective adsorbent for adsorptive removal of Malachite Green from aqueous solution, Water Conserv. Sci. Eng., 1 (2016) 69–81. doi: WCSE-D-16-00003R1
[35] W.J. Weber, J.C. Morris, Kinetics of adsorption on carbon from solution, J. Sanit. Eng. Div., 89 (1963) 31–60.
[36] Z. Bekçi, C. Özveri, Y. Seki, K. Yurdakoç, Sorption of malachite green on chitosan bead, J. Hazard. Mater., 154 (2008) 254–261.
[37] T. Santhi, S. Manonmani, T. Smitha, Removal of malachite green from aqueous solution by activated carbon prepared from the epicarp of *Ricinus communis* by adsorption, J. Hazard. Mater., 179 (2010) 178–186.
[38] B.K. Nandi, A. Goswami, M.K. Purkait, Adsorption characteristics of brilliant green dye on kaolin, J. Hazard. Mater., 161 (2009) 387–395.
[39] L. Ai, Y. Zeng, Hierarchical porous NiO architectures as highly recyclable adsorbents for effective removal of organic dye from aqueous solution, Chem. Eng. J., 215–216 (2013) 269–278.
[40] S. Ghorai, A.K. Sarkar, A.B. Panda, S. Pal, Effective removal of Congo red dye from aqueous solution using modified xanthan gum/silica hybrid nanocomposite as adsorbent, Bioresour. Technol., 144 (2013) 485–491.
[41] N.P. Raval, P.U. Shah, D.G. Ladha, P.M. Wadhwani, N.K. Shah, Comparative study of chitin and chitosan beads for the adsorption of hazardous anionic azo dye Congo Red from wastewater, Desal. Wat. Treat., 57 (2016) 9247–9262.
[42] Y. Shang, J. Zhang, X. Wang, R. Zhang, W. Xiao, S. Zhang, R. Han, Use of polyethyleneimine-modified wheat straw for adsorption of Congo red from solution in batch mode, Desal. Wat. Treat., 57 (2016) 8872–8883.
[43] T. Hao, X. Rao, Z. Li, C. Niu, J. Wang, X. Su, Synthesis of magnetic separable iron oxide/carbon nanocomposites for efficient adsorptive removal of Congo red, J. Alloys Compd., 617 (2014) 76–80.
[44] X. Yang, Z. Wang, M. Jing, R. Liu, L. Jin, X. Shen, Efficient removal of dyes from aqueous solution by mesoporous nanocomposite Al_2O_3/Ni0.5Zn0.5Fe_2O_4 Microfibers, Water. Air. Soil Pollut., 225 (2013) 1–12.
[45] H.-Y. Zhu, Y.-Q. Fu, R. Jiang, J.-H. Jiang, L. Xiao, G.-M. Zeng, S.-L. Zhao, Y. Wang, Adsorption removal of congo red onto magnetic cellulose/Fe_3O_4/activated carbon composite: equilibrium, kinetic and thermodynamic studies, Chem. Eng. J., 173 (2011) 494–502.
[46] H. Zhu, M. Zhang, Y. Liu, L. Zhang, R. Han, Study of congo red adsorption onto chitosan coated magnetic iron oxide in batch mode, Desal. Wat. Treat., 37 (2012) 46–54.
[47] Y. Yao, S. Miao, S. Liu, L.P. Ma, H. Sun, S. Wang, Synthesis, characterization, and adsorption properties of magnetic Fe_3O_4@ graphene nanocomposite, Chem. Eng. J., 184 (2012) 326–332.
[48] S. Karthikaikumar, M. Karthikeyan, K. Satheesh Kumar, Removal of congo red dye from aqueous solution by polyaniline-montmorrillonite composite, Chem. Sci. Rev. Lett., 2 (2014) 606–614.

Supplementary Material

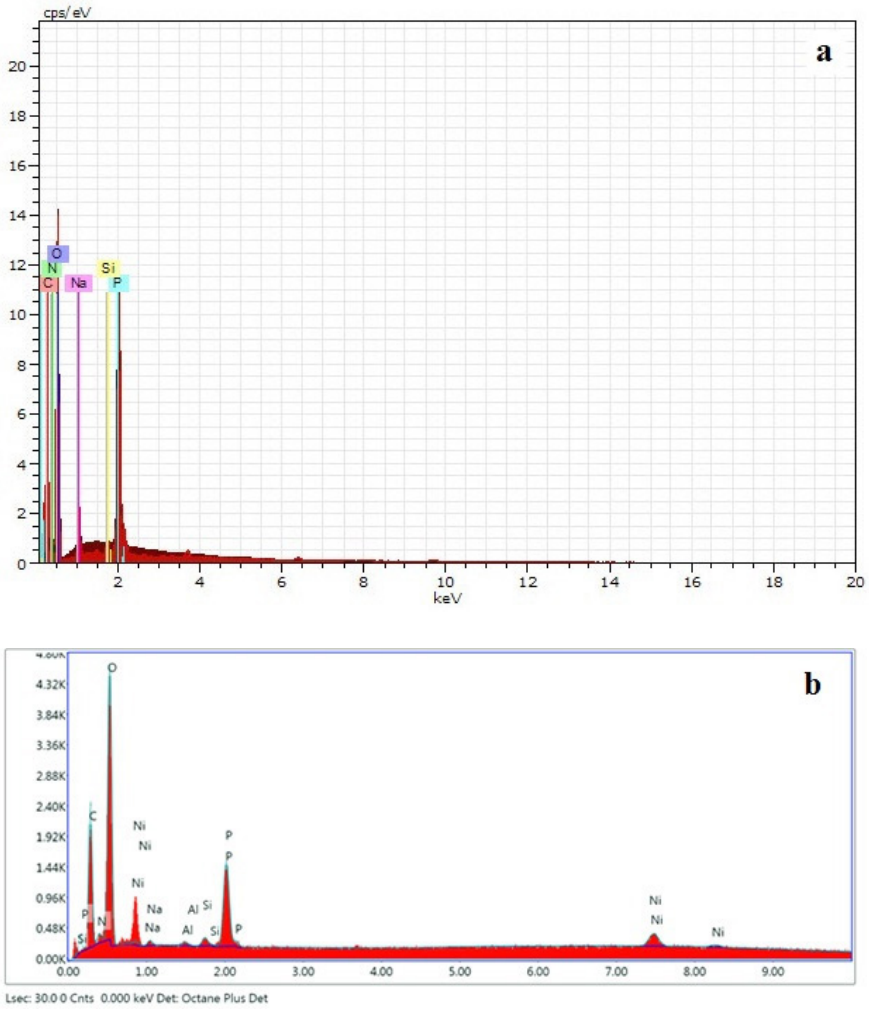

Fig. S1(a). Energy Dispersive X-ray (EDX) spectra of CTS beads. (b) Energy Dispersive X-ray (EDX) spectra of nanocomposite [CTS/NiO NPs].

Table T1
Elemental composition of chitosan beads

Element	Series	unn. C (wt.–%)	norm. C (at.–%)	Atom. C (%)	Error
Carbon	K–Series	14.66	14.66	18.86	4.7
Nitrogen	K–Series	9.76	9.76	10.77	3.2
Phosphorus	K–Series	5.07	5.07	2.53	0.2
Sodium	K–Series	0.83	0.83	0.56	0.1
Silicon	K–Series	0.00	0.00	0.00	0.0
Oxygen	K–Series	69.67	69.67	67.28	21.2

Table T2
Elemental composition of nickel oxide nanoparticles (NiO NPs)

Element	Weight %	Atomic %	Net Int.	Error %	K ratio	Z	R	A	F
C K	11.19	29.94	68.03	12.38	0.03	1.24	0.87	0.23	1
N K	1.56	3.58	9.72	25.44	0.00	1.21	0.88	0.25	1
O K	12.68	25.45	254.13	8.83	0.06	1.18	0.89	0.4	1
ClK	0.63	0.57	21.53	27.62	0.01	1	0.97	0.85	1.01
NiK	73.94	40.46	430.53	4.83	0.68	0.91	1.02	1	1

Table T3
Elemental composition of nanocomposite (CTS/NiO NPs)

Element	Weight %	Atomic %	Net Int.	Error %	K ratio	Z	R	A	F
C K	30.24	46.05	130.12	10.63	0.09	1.1	0.94	0.27	1
N K	3.77	4.92	9.72	23.41	0.01	1.08	0.96	0.17	1
O K	30.96	35.39	276.22	9.48	0.10	1.05	0.97	0.3	1
P K	9.63	5.69	233.83	4.93	0.07	0.91	1.02	0.85	1
S K	0.12	0.07	2.83	62.18	0.00	0.93	1.02	0.86	1
Ni K	25.28	7.88	86.58	12.61	0.20	0.79	1.05	1.01	1